Vertically scanned laser sheet microscopy

Di Dong,[a] Alicia Arranz,[b] Shouping Zhu,[c] Yujie Yang,[a] Liangliang Shi,[a] Jun Wang,[d] Chen Shen,[c] Jie Tian,[a,*] and Jorge Ripoll[e,f,g,*]
[a]Chinese Academy of Sciences, Key Laboratory of Molecular Imaging, Beijing 100190, China
[b]Swiss Federal Institute of Technology (ETH-Zurich), Institute for Biomedical Engineering, Switzerland
[c]Xidian University, Xian, School of Life Science and Technology, Shaanxi 710071, China
[d]Harbin University of Science and Technology, School of Automation, Harbin 150080, China
[e]Universidad Carlos III of Madrid, Department of Bioengineering and Aerospace Engineering, Madrid 28911, Spain
[f]Instituto de Investigación Sanitaria del Hospital Gregorio Marañón, Experimental Medicine and Surgery Unit, Madrid 28007, Spain
[g]Foundation for Research and Technology-Hellas, Institute of Electronic Structure and Laser, Heraklion 71110, Greece

Abstract. Laser sheet microscopy is a widely used imaging technique for imaging the three-dimensional distribution of a fluorescence signal in fixed tissue or small organisms. In laser sheet microscopy, the stripe artifacts caused by high absorption or high scattering structures are very common, greatly affecting image quality. To solve this problem, we report here a two-step procedure which consists of continuously acquiring laser sheet images while vertically displacing the sample, and then using the variational stationary noise remover (VSNR) method to further reduce the remaining stripes. Images from a cleared murine colon acquired with a vertical scan are compared with common stitching procedures demonstrating that vertically scanned light sheet microscopy greatly improves the performance of current light sheet microscopy approaches without the need for complex changes to the imaging setup and allows imaging of elongated samples, extending the field of view in the vertical direction. © 2014 Society of Photo-Optical Instrumentation Engineers (SPIE) [DOI: 10.1117/1.JBO.19.10.106001]

1 Introduction

Light sheet microscopy techniques such as selective plane illumination microscopy (SPIM)[1,2] and ultramicroscopy[3] are high-resolution volumetric fluorescence microscopic techniques which use a sheet of light to obtain optically sectioned images of biomedical samples and small specimens, with low phototoxicity and high image acquisition speeds.[4,5]

Single-sided SPIM is a simple light sheet microscopy approach which uses light sheet illumination from one side of the sample where the observation is orthogonal to the illumination plane.[6–8] Although single-sided SPIM is easy to build, the one-direction illumination scheme is sensitive to absorption, refraction, and scattering. Figure 1(a) shows an example of a single-sided SPIM where the sample is illuminated with a sheet of light collimated in the y-direction. The camera is focused through a microscope objective onto the plane generated by the light sheet with a given field of view (FOV). As shown in Figs. 1(a) and 1(b), absorption and scattering of the light sheet due to impurities or high absorbing/scattering regions in the sample result in stripes in the data due to alterations of the intensity and direction of the excitation source.[6] Moreover, inhomogeneous intensity distribution of the light source also causes stripes.

To overcome the stripe artifacts, several "stripe-eliminating" algorithms have been suggested. Münch et al. have proposed a filter based on combined wavelet and Fourier analysis, successfully reducing stripe artifacts in focused ion beam nanotomography.[9] Leischner et al., on the other hand, used non-linear horizontal smoothing to reduce the horizontal stripes in

ultramicroscopy images.[10] Fehrenbach et al. have developed an algorithm to remove stationary noise termed a variational stationary noise remover (VSNR), considering stripe artifacts as a stationary stochastic process and estimating their distribution.[11] Even though the above-mentioned methods reduce stripe artifacts, there is still room for improvement. (An example of VSNR is shown in Fig. 7). Besides these algorithms, many hardware modifications on the SPIM systems have been presented to reduce artifacts, such as multiview SPIM (mSPIM) and the use of galvo-mirrors that pivot the light sheet.[12] In addition, Fahrbach et al. have developed a holographically shaped, scanned Bessel beam to reduce scattering artifacts and increase image quality in light sheet microscopy.[13] Moreover, structured illumination and HiLo background rejection methods have also been developed.[14] Although mSPIM, beam shaping, and structured illumination greatly diminish the stripe artifacts, they increase the alignment requirements of the system and require additional hardware. Additionally, whenever several views are acquired there is an added complexity of the use markers to register the different views in order to accurately determine the axis of rotation.[15] Therefore, novel approaches are required in order to benefit from the single-sided SPIM simplicity without giving up the quality of the images obtained.

In this paper, a vertical-scanning method is introduced to reduce the above-mentioned stripes in light sheet microscopy making use of the basic components of an SPIM system. We classified the stripes into two groups: motionless stripes and moving stripes. We assume that the motionless stripes are caused by the inhomogeneous illumination and impurities that might be present outside the sample, and as shown in Fig. 1(c),

---

*Address all correspondence to: Jie Tian, E-mail: tian@ieee.org; Jorge Ripoll, E-mail: jorge.ripoll@uc3m.es
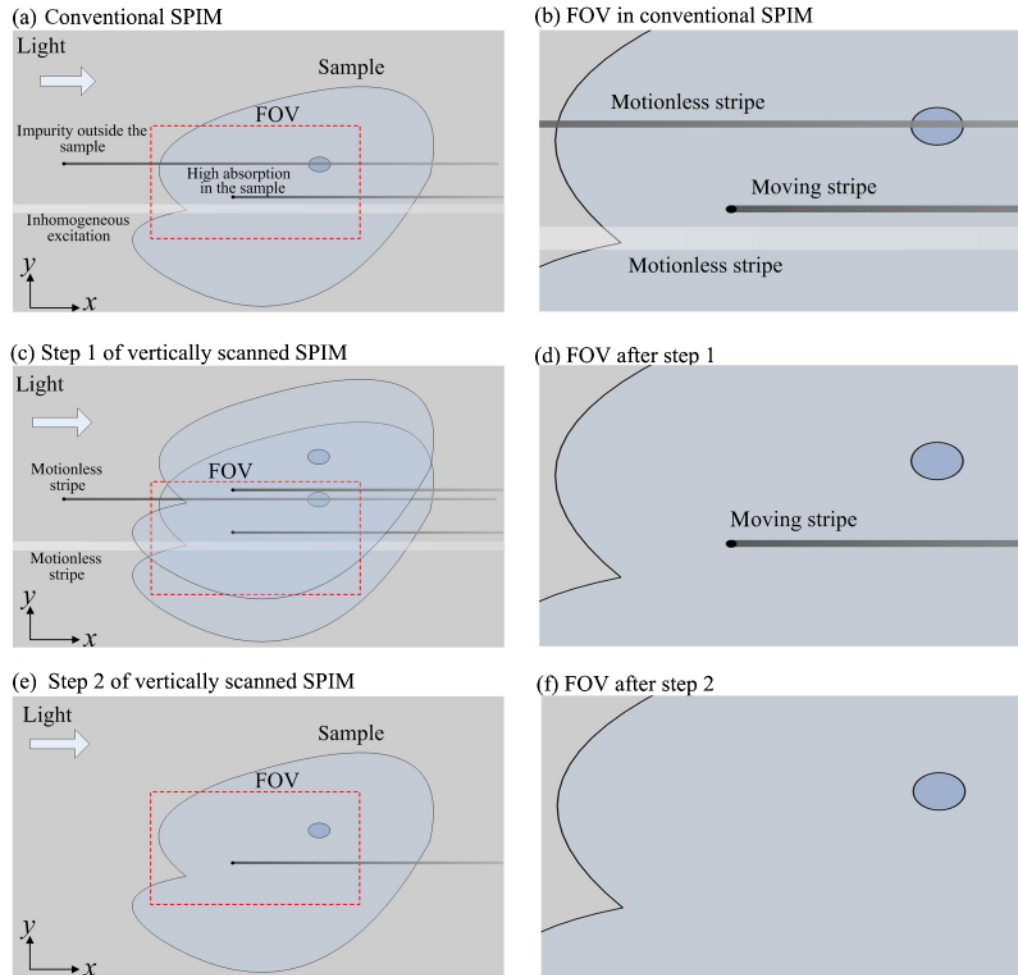
Fig. 1 The scheme of the proposed vertically scanned selective plane illumination microscopy (SPIM). (a) The typical stripe artifacts in conventional single-sided SPIM. (b) Field of view (FOV) in the conventional SPIM. (c) Step 1 of vertically scanned SPIM. (d) FOV after step 1 of vertically scanned SPIM. (e) Step 2 of vertically scanned SPIM. (f) FOV after step 2 of vertically scanned SPIM.

they do not move synchronously when displacing the sample vertically. In contrast, the moving stripes are caused by the high absorbing/scattering structures inside the sample and move together with the sample. Both types of stripes will significantly degrade the light sheet microscopy image as shown in Fig. 1(b). With the approach we present here, we utilize two steps to remove these stripes. In the first step, we vertically scan the sample during the imaging acquisition process and then merge the overlapping images into one single image. Since the motionless stripes do not move synchronously with the sample, this step effectively reduces motionless stripes and improves image quality. The second step uses the VSNR method to further reduce the remaining moving stripes. The experimental results show that the combination of the two procedures results in a significant image quality improvement.

This paper is organized as follows. Section 2 presents how the sample is prepared for imaging, while Sec. 3 gives details of the experimental setup and acquisition procedure. Section 4 introduces our method in detail, presenting two comparative experiments on a mouse colon with conventional stitching-SPIM and the VSNR method, respectively. Results, conclusions, and future work are shown in Secs. 5 and 6.

2 Sample Preparation

All procedures described here were approved by the Veterinary Department of the Heraklion Prefecture (Heraklion, Crete, Greece). Mice were housed at the animal facility in the School of Medicine, University of Crete. Animals were kept in standard housing conditions providing water and food *ad libitum*. Prior to collection of tissue samples, animals were deeply anesthetized and euthanized. Colon tissue was aseptically removed, washed, and flushed with phosphate buffer solution (PBS) and fixed in 4% paraformaldehyde (PFA) for at least 24 h at 4°C. After fixation, samples were washed twice with PBS, incubated with 1% weight/vol Triton X-100 for 30 min and washed again with PBS prior to staining. Single staining with propidium iodide (30 μg/ml in PBS; Sigma-Aldrich, St. Louis, Missouri) was performed at room temperature for 30 min in the dark followed by three washes with PBS of 10 min each.

Once the staining procedure was completed, samples were mounted in 1.3% low-melting agarose (SeaPlaque, Lonza Rockland Inc., Rockland, Maine). Mounted samples were then dehydrated by successive washes through a graded series of methanol (25%, 50%, 75%, and 100%; 1 h/wash) and left in

100% methanol overnight. Mounted samples were then transferred to benzyl alcohol and benzyl benzoate (BABB in a 1:2 ratio; Sigma-Aldrich) for at least 24 h. Measurements were performed with the samples submerged in a glass cuvette filled with BABB.

3 Laser Sheet Microscopy Setup and Data Acquisition

Once we had the tissue sections cleared, stained, and mounted in agarose, we immersed them in a vessel of matching liquid, BABB in this case. Movement of the sample took place by attaching the end of the agarose block to a group of stages which provide rotation and translation movement in the x-, y-, and z-directions. A light sheet was generated by a 473 nm laser (Roithner LaserTechnique, Vienna, Austria) focused through a cylindrical lens of focal length $f = 10$ mm and a $10\times$ infinity corrected objective (Mitutoyo, Kawasaki, Japan). A $5\times$ infinity corrected objective (Mitutoyo, Kawasaki, Japan) with a 525-nm bandpass fluorescence filter with ±17.5-nm width, a tube lens and a thermoelectric cooled intensified CCD camera (iXon DV885 ANDOR Technology, Belfast, Northern Ireland, 1004×1002 pixels, 8×8 μm pixel size, using 2×2 binning) were used for detection. Further details of the SPIM setup used in this work can be found in Ref. 16.

As mentioned previously, the vertically scanned light sheet microscope was used to image a cleared mouse colon stained with propidium iodide mounted in a block of agarose. For the sample shown, we acquired 2902 patches for the vertically scanned SPIM (99% overlap) and 30 patches for the conventional stitched-SPIM method (5% overlap). With regards to motor displacement, note that for higher magnifications the accuracy of the motor might play a role on the resolution of the images. In all data presented here, the effect of the step resolution of our motors (~1 μm) was negligible for the magnification used ($5\times$, with the pixel size of ~8 μm) and we found it started to play a role only when using a $50\times$ objective and higher.

4 Stripe Removal Method

To remove the stripe artifact present in SPIM, we propose a method which consists of two steps: (1) acquiring vertically scanned images and fusing them together and (2) using the VSNR method to reduce the remaining stripes in the complete image. The scheme of our method is shown in Figs. 1(c)–1(f). Step 1 is schematically represented in Figs. 1(c) and 1(d), where we show that by acquiring several vertical displacements with strong overlap while recording the movement of the translation stage with high accuracy, we can effectively suppress the motionless stripes caused by both the impurities outside the sample and the inhomogeneous intensity distribution of the light source. However, as shown in Fig. 1(d), there might still be moving stripes retained in the image after step 1. These moving stripes are caused by the highly absorbing and/or scattering areas inside the sample and, therefore, move synchronously with the sample. In order to remove the remaining stripes, we use VSNR as step 2 to further reduce these remaining stripes [see Figs. 1(e) and 1(f)]. The results show that the combination of the two steps can effectively reduce the stripes and improve the image quality. In the following paragraphs, we will introduce the implementation of the two steps in detail.

4.1 Vertical Scanning of the Sample

Figure 2 shows a simplification of step 1. Using the detection setup shown in Sec. 3, each view covered a 3.8×3.8 mm region in the FOV; from now on we shall term this FOV a "patch," since it does not cover the whole sample in the focal plane. By fusing a collection of patches, we may recover the full image either through stitching (images acquired with slightly overlapping FOVs, 5% to 20% typically),[17] or by fusing vertically scanned patches (images acquired with almost 99% overlap). The experimental procedure consisted of translating the sample to an initial position where the top of the sample was visible. Then, by applying a constant speed to the vertical translation while continuously acquiring images, we collected a stack of patches.
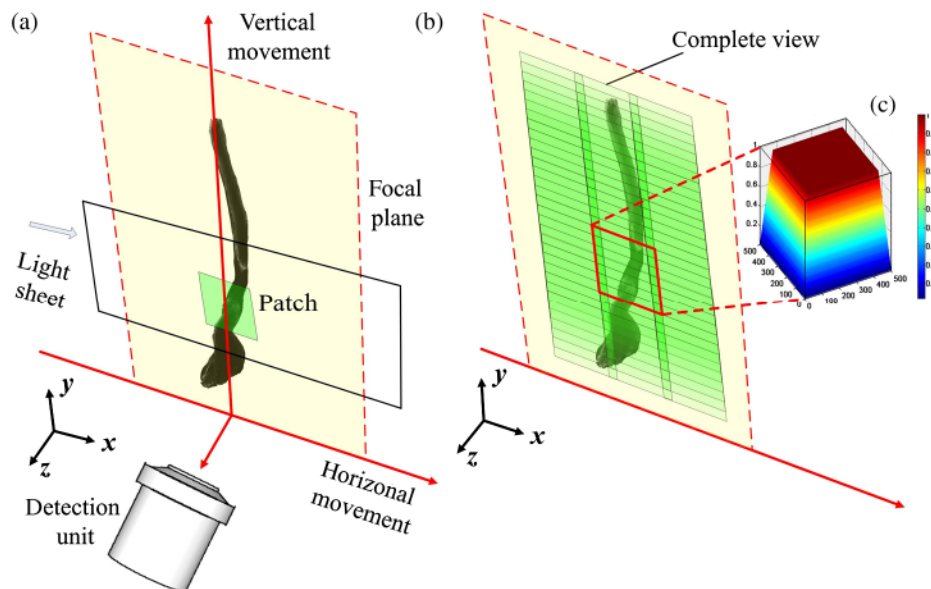

Fig. 2 Step 1 of vertically scanned light sheet microscopy. (a) The detection unit is focused on a part of the sample in the focal plane. A single image is called a patch. (b) All overlapped patches are fused together taking into account the speed of the vertical translation stage to form an image of the complete sample in the focal plane. (c) The weighting mask of a patch for interpolation.

In the case shown here, the vertical speed was about 0.3 mm/s, roughly a 30 μm displacement between images, showing a 99% degree in overlap between images. Specifically for the case presented here, additional measurements for x (lateral) positions (3 in total, with 20% overlap) were needed in order to cover the complete span of the sample [see Fig. 2(b)]. The video recording of patch images from 200th to 475th are shown in Video 1. Figure 3 shows several frames in Video 1, where we show the same region in different patch images. It can be seen that there is a severe motionless stripe whose movement is not synchronized with the sample. This stripe is caused by a high absorbing impurity outside the sample, possibly present in the cuvette.

After data acquisition, all the patches were fused together with our reconstruction method to form a stitched view. Our reconstruction method includes two substeps: (1) before the interpolation, the total size of the stitched view was calculated according to the recorded x and y positions of the patches and (2) all of the patches were included in the stitched view and the overlapping regions were substituted by weighted averages of all those patches which covered that specific region. As shown in Fig. 2(c), a flat-topped pyramid was chosen as the weighting mask of each patch to smooth the junctions of different patches. The maximum of the weighting mask was set to 1, while the weights descended from 1 to 0 at the boundary of the mask (30 pixels). By using such a mask, the boundary of each patch has a small contribution to the final view, which suppresses the line gaps at the junctions between two patches. Step 1 can remove the motionless stripes and produce a stitched SPIM image. However, it fails to suppress the moving stripe. Therefore, we perform step 2 to further reduce these moving stripes.

With respect to the effect on acquisition times of the vertical displacement, it should be pointed out that the acquisition time of SPIM is related to the mode of data acquisition and sample movement. Conventional SPIM can be divided into two types: continuous translation SPIM and intermittent translation SPIM. In continuous translation SPIM, the sample moves with a constant-velocity translation and images are collected simultaneously with the movement. The exposure time per image in our method is equivalent to that of conventional continuous translation SPIM since the exposure time is determined mainly by the brightness of the fluorescent dyes or fluorescent proteins in the sample. Furthermore, the exposure time determines the moving speed of the sample to be used in continuous translation SPIM in order to avoid blurring of the images due to movement. Therefore, the translation speed and the total acquisition times of our method are also equivalent with conventional continuous translation SPIM, the main difference being that our method has shorter time delays between acquisitions. In intermittent translation SPIM, the sample moves in a move-stop-move mode and the image acquisition only happens when the sample stops. As in the previous case, the exposure time of a single image in intermittent translation SPIM is given by the brightness of the sample. In this case, however, significant time is consumed in moving and stabilizing the motors before image collection, slowing down the data acquisition process and yielding, on average, equivalent or even higher overall exposure times, depending on the quality of the motors. In summary, while testing all three approaches, we found that our method effectively removed the stripes without significantly increasing the acquisition time.

4.2 Variational Stationary Noise Remover Method

Once the static stripes are removed using the vertically scanned measurements, we implement step 2 based on the VSNR method.[11] The VSNR method regards the noise in an image (e.g., the stripes, Poisson or Gaussian white noise) as stationary noise and describes them with different noise elements. In the VSNR method, several noise elements are first selected manually according to the noise type present in the image. Then, a restoration method based on maximum a posteriori is used to estimate the noise distributions and effectively remove them. Details of its implementation can be found in Ref. 11.

In step 2 of our approach, we applied VSNR to reduce the remaining stripes which survived step 1. We choose an anisotropic Gabor element ψ as the stripe noise element. Note that this filter element will depend mainly on the illumination objective and the magnification of the system, being equivalent when measurements are taken under similar experimental conditions. Our goal is to find a distribution λ of the stripe distribution. The stripe image is denoted as $u_s = \lambda * \psi$, where * denotes convolution. If we denote the stitched image in step 1 as u and consider that there are only stripe artifacts
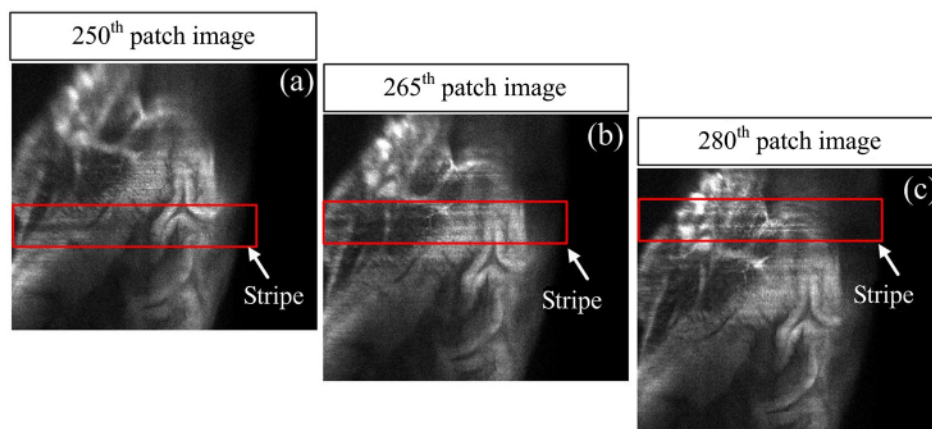

Fig. 3 Several frames selected from Video 1 (AVI, 3.8 MB) [URL: http://dx.doi.org/10.1117/1.JBO.19.10.106001.1]. (a) The 250th patch image. (b) The 265th patch image. (c) The 280th patch image.
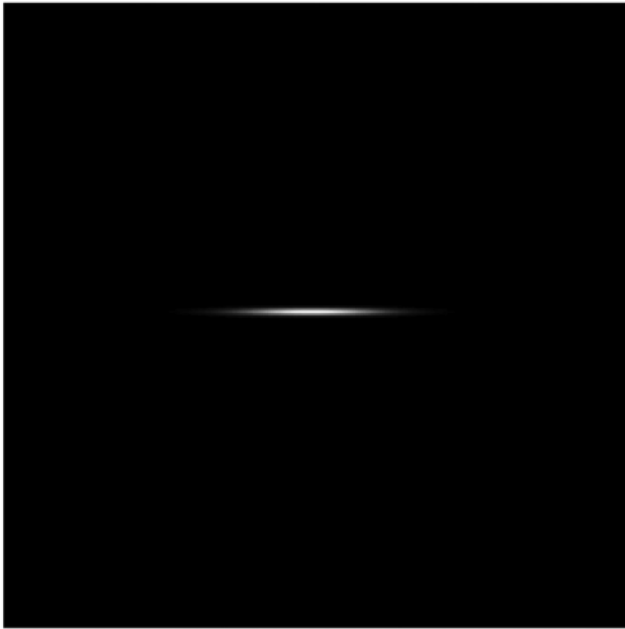
Fig. 4 The Gabor element used in step 2 for image restoration.

left in the stitched image, the total image would be $u = u_0 + u_s$, where u_0 is the image without stripe artifacts. At this point, we perform an interactive optimization process to estimate λ. Given ψ and u, in each loop, we use an updated λ to estimate u_s. We then calculate u_0 and calculate a relative change when compared with the result from the previous loop. If the relative change is less than a precision or the number of iterations exceeds a default number, the loop stops and outputs current u_0. Otherwise, we update λ and run the next loop. Detailed implementation of this approach and the selection of the Gabor element can be found in Ref. 11.

Considering our experimental data and the resulting stitched SPIM image, the orientation of the Gabor element in our case is horizontal, which the result of the orientation of the stripes. The width and length of the Gabor element for this particular case were chosen to be 11 and 201 pixels, respectively. The default number of iterations was set to 100 and the precision to 0.005. Figure 4 shows the Gabor element for the results presented here. As mentioned previously, each experimental configuration will have its own optimal Gabor filter, given by the orientation and width of the stripe artifacts.

5 Results

The performance of step 1 and step 2 is shown in Fig. 5. As shown in Figs. 5(a) and 5(b), there are several stripes present in the collected patch images. As shown in Figs. 5(c) and 5(d), most of the motionless stripes are removed and the image quality is greatly enhanced after step 1. However, there are still a few remaining stripes, specifically those which move synchronously with the sample and are caused by high absorbing/scattering regions inside the sample. Step 2 is shown in Figs. 5(e)–5(h), where 5(e) and 5(f) show the stripe images extracted through the implementation of the VSNR method in step 2, and 5(g) and 5(h) represent the final results. It can be seen that step 2 eliminates the remaining stripes from step 1. In conclusion, the combination of step 1 and step 2 results in the stripes' suppression and image quality improvement.

The results with and without vertically scanned SPIM are shown in Fig. 6, where 6(a) shows the stitched SPIM images and 6(b) shows the same region making use of the vertically scanned method. Figures 6(c) and 6(e) show two zoomed images obtained with conventional stitching where the stripes are clearly visible. In contrast, using the vertically scanned approach, the stripe artifacts are greatly reduced [see Figs. 6(d) and 6(f)]. The vertical-scanning approach also reduces the noise [see in Figs. 6(g) and 6(h)] and provides good detail compared to images obtained with the conventional stitching of SPIM images [see Figs. 6(i) and 6(j)].

In order to further evaluate the performance of our two-step method, we compared it with the combination of conventional
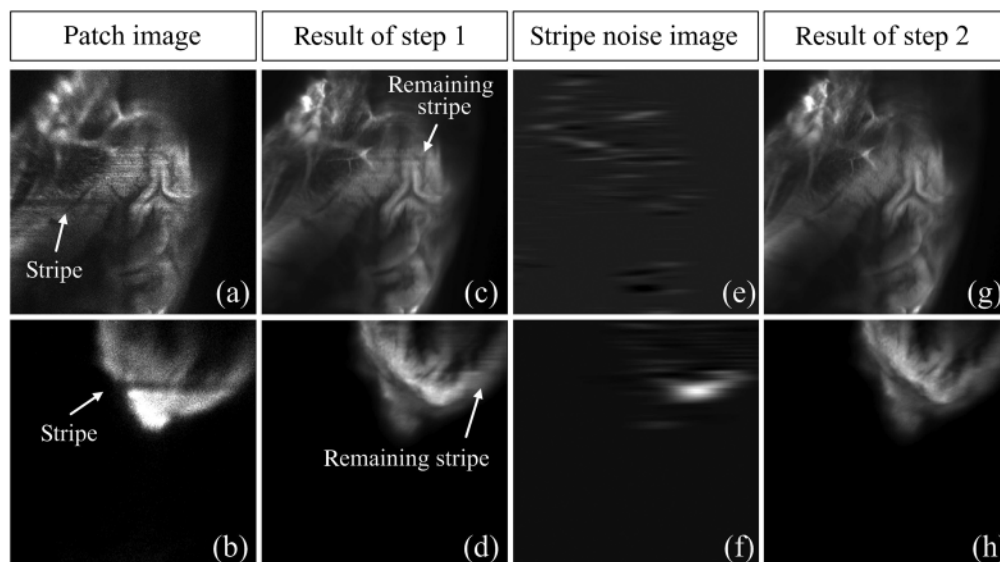

Fig. 5 The results of each step in our method. (a and b) Two raw patch images acquired by our system. (c and d) The results of step 1. (e and f) The stripe artifacts extracted by step 2. (g and h) The results of implementing step 2.
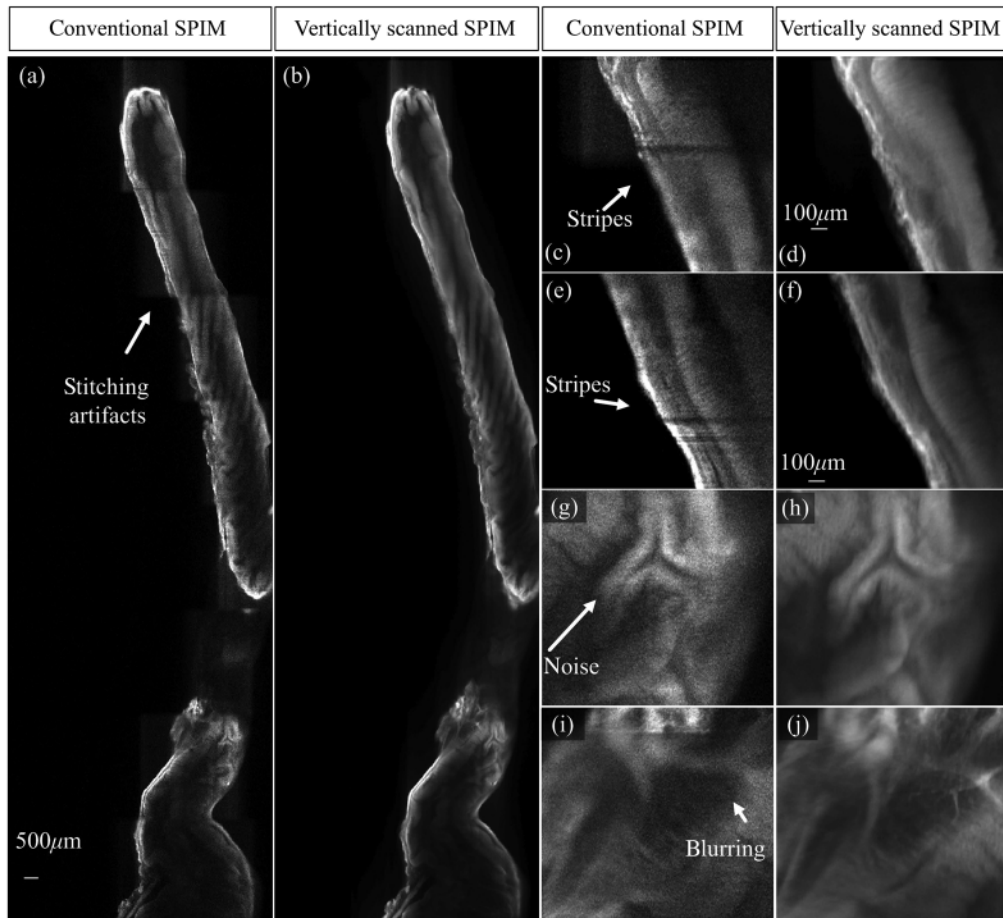
Fig. 6 Comparison results between our method and conventional stitching-SPIM on images from a mouse colon. (a) Whole organ image with conventional stitched-SPIM method and (b) with our vertically scanned SPIM method. (c), (e), (g), and (i) Zoomed images with conventional stitched-SPIM method. (d), (f), (h), and (j) Zoomed images with the vertically scanned SPIM method.
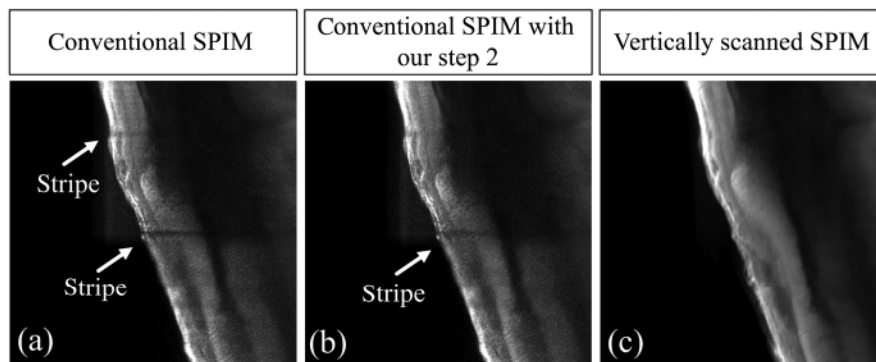

Fig. 7 Comparison results between conventional SPIM, conventional SPIM with step 2, and our method on a serious stripe. (a) The result of conventional SPIM. (b) The result of conventional SPIM with step 2. (c) The result of our vertically scanned SPIM.

stitched-SPIM and VSNR. As shown in Figs. 7(a) and 7(b), VSNR (as in step 2) failed to eliminate the stripes from the image obtained by conventional SPIM. In contrast, as shown in Fig. 7(c) vertically scanned SPIM combined with VSNR results in a stripe-free image, highlighting the fact that vertically scanning the sample prior to VSNR greatly enhances the image quality.

6 Conclusions

In this study, a vertically scanned scheme was proposed to reduce stripes, noise and scattering effects in light sheet microscopy images. This approach can be easily applied to a conventional single-side SPIM setup by including a high-resolution vertical translation stage with a travel range larger than the target area. The experimental results shown here illustrate that the

image quality of the conventional SPIM is indeed improved when using our two-step vertically scanned method. Moreover, the vertically scanned light sheet microscopy also improves the image quality in those cases presenting inhomogeneous light sheet illumination. Note, however, that this improved image quality also implies that each section imaged receives a larger amount of laser power and is thus more susceptible to photobleaching, since while the sample is translated vertically the same area is exposed as it traverses the FOV. However, we believe that the strength of our approach lies in the fact that our vertically scanned laser sheet microscopy presents a way to observe large elongated samples seamlessly by allowing the enlargement of the FOV in the vertical direction while simultaneously improving image quality. This increase in FOV makes our method suitable for bowel imaging, spinal cord imaging, and general imaging of elongated samples.

Although only two-dimensional results are shown here, three-dimensional overlapping imaging can be easily implemented by including sample translation in the optical axis as in conventional SPIM. Furthermore, multiview vertically scanned SPIM can also be obtained by combining mSPIM[18] with the vertical scan proposed here. We believe that including this scheme in current light sheet microscopes will further increase their capabilities by imaging elongated samples while simultaneously reducing SPIM artifacts.

Acknowledgments

References

1. J. Huisken et al., "Optical sectioning deep inside live embryos by selective plane illumination microscopy," *Science* **305**(5686), 1007–1009 (2004).
2. J. Huisken and D. Y. R. Stainier, "Selective plane illumination microscopy techniques in developmental biology," *Development* **136**(12), 1963–1975 (2009).
3. H.-U. Dodt et al., "Ultramicroscopy: three-dimensional visualization of neuronal networks in the whole mouse brain," *Nat. Methods* **4**(4), 331–336 (2007).
4. P. J. Keller et al., "Reconstruction of zebrafish early embryonic development by scanned light sheet microscopy," *Science* **322**(5904), 1065–1069 (2008).
5. O. Olarte et al., "Image formation by linear and nonlinear digital scanned light-sheet fluorescence microscopy with Gaussian and Bessel beam profiles," *Biomed. Opt. Express* **3**(7), 1492–1505 (2012).
6. M. Weber and J. Huisken, "Light sheet microscopy for real-time developmental biology," *Curr. Opin. Genet. Dev.* **21**(5), 566–572 (2011).
7. D. Turaga and T. Holy, "Aberrations and their correction in light-sheet microscopy: a low-dimensional parametrization," *Biomed. Opt. Express* **4**(9), 1654–1661 (2013).
8. Y. Wang, X. Ji, and Q. Dai, "Key technologies of light field capture for 3D reconstruction in microscopic scene," *Sci. China Inf. Sci.* **53**(10), 1917–1930 (2010).
9. B. Münch et al., "Stripe and ring artifact removal with combined wavelet—Fourier filtering," *Opt. Express* **17**(10), 8567–8591 (2009).
10. U. Leischner et al., "Formalin-induced fluorescence reveals cell shape and morphology in biological tissue samples," *PLoS One* **5**(4), e10391 (2010).
11. J. Fehrenbach, P. Weiss, and C. Lorenzo, "Variational algorithms to remove stationary noise: applications to microscopy imaging," *IEEE Trans. Image Process.* **21**(10), 4420–4430 (2012).
12. J. Huisken and D. Y. R. Stainier, "Even fluorescence excitation by multidirectional selective plane illumination microscopy (mSPIM)," *Opt. Lett.* **32**(17), 2608–2610 (2007).
13. F. Fahrbach, P. Simon, and A. Rohrbach, "Microscopy with self-reconstructing beams," *Nat. Photonics* **4**(11), 780–785 (2010).
14. T. Schröter et al., "Scanning thin-sheet laser imaging microscopy (sTSLIM) with structured illumination and HiLo background rejection," *Biomed. Opt. Express* **3**(1), 170–177 (2012).
15. S. Preibisch et al., "Software for bead-based registration of selective plane illumination microscopy data," *Nat. Methods* **7**(6), 418–419 (2010).
16. A. Arranz et al., "Helical optical projection tomography," *Opt. Express* **21**(22), 25912–25925 (2013).
17. A. Ertürk et al., "Three-dimensional imaging of the unsectioned adult spinal cord to assess axon regeneration and glial responses after injury," *Nat. Med.* **18**(1), 166–171 (2011).
18. J. Swoger et al., "Multi-view image fusion improves resolution in three-dimensional microscopy," *Opt. Express* **15**(13), 8029–8042 (2007).

Di Dong received his BS degree in automation from the University of Science and Technology, Beijing, in 2008, and his PhD degree in pattern recognition and intelligent systems from the Institute of Automation, Chinese Academy of Sciences, in 2013. He is an assistant professor at the Institute of Automation, Chinese Academy of Sciences. His current research interests include selective plane illumination microscopy and optical projection tomography.

Alicia Arranz obtained her PhD in biology from the UCM (Spain) in 2008, and has been awarded with several international fellowships (MICINN-Fullbright and Marie Curie IEF) having worked in different prestigious international institutions (such as UCLA in Los Angeles, Tuft's University in Boston and the ETH in Zurich). She recently joined the Center for Molecular Biology (Spain). Her current interests lie in developing new methodologies for imaging inflammation and immune response.

Shouping Zhu received the BS degree and the MS degree from Xidian University, Xi'an, China, in 2004 and 2007, respectively, and received the PhD degree from Institute of Automation, Chinese Academy of Sciences, Beijing, China, in 2010. He has been with the School of Life Science and Technology, Xidian University, since 2010, where he is currently an associate professor. His research interest covers micro-CT imaging, optical imaging, and multimodality fusion.

Yujie Yang is a master's student in the Key Laboratory of Molecular Imaging, Institute of Automation, Chinese Academy of Sciences, Beijing 100190, China. She received the BE degree from Beihang University, in 2012. Her research interests are mainly focused on optical imaging.

Liangliang Shi is a master's student in the Key Laboratory of Molecular Imaging, Chinese Academy of Sciences, Beijing 100190, China. He received the BE degree from North China Electric Power University, in 2012. His research interests are mainly focused on optical projection tomography and multimodality molecular imaging.

Jun Wang has been a master's student in the School of Measurement–Control Technology and Communications Engineering of Harbin University of Science and Technology since September 2013. He received the BE degree from Pingdingshan University. Since March 2014, as a visiting student, he has studied in the Key Laboratory of Molecular Imaging, Chinese Academy of Sciences, Beijing 100190. His research interests are mainly focused on Optical Projection Tomography and Multimodality Molecular Imaging.

Chen Shen was graduated with a degree in applied physics from the University of Central Lancashire, in 2010. He received his master of science in computational physics from the University of Edinburgh, in 2012, supervised by Edinburgh Parallel Computing Centre (EPCC, UK's National Supercomputer Centre). He is currently a PhD student under the direction of Prof. Tian Jie, mainly engaged in the study of microscopic neuroimaging.

Jie Tian received the PhD degree in artificial intelligence from the Institute of Automation, Chinese Academy of Sciences, Beijing, China, in 1992. From 1995 to 1996, he was a postdoctoral fellow with the Medical Image Processing Group, University of Pennsylvania, Philadelphia. Since 1997, he has been a professor with the Intelligent Medical Research Center, Institute of Automation. His current research interests include medical image process and molecular imaging.

Jorge Ripoll obtained his PhD in physics from the UAM (Spain) in 2000, in close collaboration with UPENN (USA), UCL (England), and MGH-Harvard (USA). He obtained tenure track positions in FORTH (2005–2012), where he led a research group for more than 7 years. Since September 2012 he has been with the Department of Bioengineering of the UC3M (Spain). He authored of "Principles of Diffuse Light Propagation" (World Sci. Press, 2012), and his current interests lie in the development of *in vivo* optical tomography approaches.